UCP2 regulates mitochondrial fission and ventromedial nucleus control of glucose responsiveness

Chitoku Toda[1,2], **Jung Dae Kim**[1,2], **Daniela Impellizzeri**[1,2,3], **Salvatore Cuzzocrea**[1,3], **Zhong-Wu Liu**[1,2], and **Sabrina Diano**[1,2,4,5,*]

[1]Program in Integrative Cell Signaling and Neurobiology of Metabolism, Yale University School of Medicine, New Haven, Connecticut, 06520 USA

[2]Department of Obstetrics, Gynecology, and Reproductive Sciences, Yale University School of Medicine, New Haven, Connecticut, 06520 USA

[3]Department of Biological and Environmental Sciences, University of Messina, Messina, 98166 Italy

[4]Department of Neurobiology, Yale University School of Medicine, New Haven, Connecticut, 06520 USA

[5]Section of Comparative Medicine, Yale University School of Medicine, New Haven, Connecticut, 06520 USA

Summary

The ventromedial nucleus of the hypothalamus (VMH) plays a critical role in regulating systemic glucose homeostasis. How neurons in this brain area adapt to the changing metabolic environment to regulate circulating glucose levels is ill-defined. Here we show that glucose load results in mitochondrial fission and reduced reactive oxygen species in VMH neurons mediated by dynamin-related peptide 1 (DRP1) under the control of uncoupling protein 2 (UCP2). Probed by genetic manipulations and chemical-genetic control of VMH neuronal circuitry, we unmasked that this mitochondrial adaptation determines the size of the pool of glucose-excited neurons in the VMH, and, that this process regulates systemic glucose homoeostasis. Thus, our data unmasked a critical cellular biological process controlled by mitochondrial dynamics in VMH regulation of systemic glucose homeostasis.

*To whom correspondence should be addressed at: Department of Obstetrics, Gynecology, and Reproductive Sciences, Yale University School of Medicine, New Haven, CT 06520, USA, Telephone: 203-737-1216. FAX: 203-785-4713. Sabrina.diano@yale.edu.

Introduction

The hypothalamus is an important site for regulation of energy- and glucose metabolism (Dietrich and Horvath, 2013; Sandoval et al., 2009). Homeostatic control of glycemic levels is pivotal not only for preventing seizures, unconsciousness and brain injury induced by hypoglycemia, but also for protecting the brain from glucose toxicity in diabetes. The ventromedial nucleus of the hypothalamus (VMH) has been recognized as a key region in the regulation of glucose metabolism (Grayson et al., 2013; Morton and Schwartz, 2011). Glucose sensing neurons of the VMH are either activated or inhibited by increased glucose levels and their responses to changes in glucose levels have been shown to be important for the counter-regulatory responses to restore euglycemia following insulin-induced hypoglycemia (Borg et al., 1994; Chan and Sherwin, 2013) and for the secretion of pancreatic insulin in response to increased glucose levels (Kim et al., 2014).

Alteration in mitochondrial dynamics, i.e. mitochondrial fission and fusion, has been observed in metabolic tissues of human and rodent models of diabetes. Whether mitochondrial dynamics in neuronal populations of the VMH is involved in control of systemic glucose homeostasis is still ill-defined.

Results

Systemic glucose load induces mitochondrial fission in VMH neurons

To test whether mitochondrial dynamics occur in VMH neurons in response to glucose, we measured mitochondrial size, density and coverage after glucose or saline administration. We found that systemic glucose administration decreased mitochondrial size (Fig. 1A) and increased mitochondrial density (Fig. 1B) in VMH neurons. However, the total mitochondrial area in the cytosol was not changed (Fig. 1C), indicating that glucose promotes mitochondrial fragmentation (Fig. S1A and B). Mitochondrial fission is regulated by dynamin-related peptide 1 (DRP1), of which active, phosphorylated form is associated with the outer membrane of mitochondria (Fig. 1D). Western blot analysis showed that glucose administration significantly increased the ratio pDRP1/DRP1 compared to saline-injected controls (Fig 1E-F) confirming glucose-induced mitochondrial fission in VMH neurons.

Activation of DRP1 is UCP2 dependent in the VMH

We have previously shown that increased mitochondria number in neuronal perikarya is promoted by UCP2 in the arcuate nucleus (Andrews et al., 2008; Coppola et al., 2007). UCP2 is also robustly expressed in the VMH (Richard et al., 1998). Thus, next we tested whether the presence of UCP2 impacts VMH DRP1 phosphorylation in response to a glucose load. To this end, we generated whole body Ucp2 knockout (*Ucp2KO*) mice and *Ucp2KO* mice with selective re-expression of UCP2 in the VMH (*Ucp2KOKI^{Sf1}*). We first generated mice in which UCP2 coding sequence with CAG promoter and a lox P floxed stop codon (LSL) were inserted into ROSA26 locus (*Ucp2KI^{fl/fl}*, Gt(ROSA26-LSL-UCP2-GFP; Suppl. Fig. 2A). *Ucp2KI^{fl/fl}* animals were crossed with *Ucp2KO* mice (*Ucp2KOKI^{fl/fl}*). These mice were then crossed with *Sf1-cre* mice (Dhillon et al., 2006). In contrast to the

increased ratio pDRP1/DRP1 in control mice, no significant changes were observed in glucose-treated *Ucp2KO* mice (Fig. 2 A). On the other hand, glucose administration to *Ucp2KO* mice with selective re-expression of UCP2 in the VMH (*Ucp2KOKI^{Sf1}* mice; Fig. S2B, D-G) significantly increased pDRP1/DRP1 ratio to levels similar to those observed in control mice (Fig. 2A). pDRP1/DRP1 ratio of saline-treated mice were comparable between the 3 groups (Fig. 2A). Furthermore, saline-injected mice with selective overexpression of UCP2 in SF1 neurons (*Ucp2KI^{Sf1}* mice; Fig. S2A, C, H-K) showed a greater pDRP1/DRP1 ratio compared to saline-treated controls (Fig. 2B), and, glucose administration to *Ucp2KI^{Sf1}* mice induced a further increase in pDRP1/DRP1 ratio compared their saline group, which was also significantly greater than that observed in glucose-treated controls (Fig. 2B). These results show that UCP2 is critical for DRP1 phosphorylation in the VMH in response to elevated glucose load.

Mitochondrial fission is UCP2 dependent in the VMH

Next we interrogated whether the control of DRP1 by UCP2 affects mitochondrial adaptations in the VMH in response to glucose. We found that the glucose administration-triggered alterations in mitochondrial size and density in SF1 positive VMH neurons were not present in *Ucp2KO* mice (Fig. 2C and D; Fig. S1C-D). On the other hand, glucose administration significantly reduced mitochondrial size while increasing mitochondrial number in VMH SF1 neurons of *Ucp2KOKI^{Sf1}* (Fig. 2F and G; Fig. S1E-F) and of *Ucp2KI^{Sf1}* mice (Fig. 2I and J; Fig. S1G and H) reaching levels similar or greater than those of control mice, respectively. No difference in mitochondrial coverage was found between groups (Fig. 2E, H and K). These results together with the findings on DRP1 phosphorylation unmasked that UCP2 promotes mitochondrial fission in the VMH in response to systemic glucose load.

Glucose-induced neuronal activation and decreased ROS production in the VMH are UCP2-dependent

We next examined the effect of glucose load on VMH neuronal activation assessed by cfos immunolabeling. Baseline c-fos labeling in saline-injected groups was similar (Fig.3 A-D). However, after peripheral glucose administration, reduced c-fos labeling in SF1 neurons was observed in the VMH of *Ucp2KO* mice (18.5±4.3 cell count/section; p=0.005) compared to controls (51.6±2.8 cell count/section; Fig. 3 E, F, I and J). On the other hand, selective re-expression of UCP2 in VMH neurons restored c-fos activation in *Ucp2KOKI^{Sf1}* mice (45.5±9.54 cell count/section; Fig. 3G and K). Furthermore, *Ucp2KI^{Sf1}* mice showed a greater increase in cfos immunoreactivity compared to control mice (87.4±12.6 cell count/ section; p=0.02; Fig. 3 H, L and M). In addition, when we analyzed the three subdivisions of the VMH, dorsomedial (dmVMH), central (cVMH) and ventrolateral (vlVMH), *Ucp2KI^{Sf1}* mice showed a significant increase in cfos staining in all divisions of the VMH (Fig. 3M).

UCP2 was shown to regulate neuronal activity, in part, by controlling ROS production (Coppola et al., 2008; Andrews et al., 2008; Diano et al., 2012). Glucose administration induced a significant elevation of ROS levels in SF1 neurons of *Ucp2KO* mice compared to controls (Fig. 3N, O and R). VMH re-expression of UCP2 was sufficient to reduce ROS to the levels observed in control mice (Fig. 3N, P and R).

Glucose administration induced a significant reduction of ROS levels also in VMH neurons of *Ucp2KI^Sf1* mice, which reduction was significantly greater than that observed in control mice (Fig. 3N, Q and R). These results indicate that UCP2 enables VMH neuronal activation in response to a glucose load, in part by reducing ROS levels.

Systemic glucose homeostasis is regulated by VMH UCP2

The VMH plays an important role in glucose metabolism. To test whether UCP2 in the VMH has relevance to systemic glucose control, we analyzed glucose homeostasis in control, *Ucp2KO,* and *Ucp2KOKI^Sf1* mice (Fig. 4). *Ucp2KO* mice displayed glucose intolerance compared to control mice (Fig. 4A). Selective re-expression of UCP2 in the VMH of *Ucp2KOKI^Sf1* mice restored glucose tolerance to a level that was not statistically different from that of control mice (Fig. 4A). No differences in circulating insulin levels were observed between groups (Fig. 4B). Furthermore, analyses of body weight (Fig. S3A) and composition (Fig. S3B-C) and histological analysis of pancreatic β-cells (Fig. S3D-H) showed no difference between groups.

To assess insulin action, hyperinsulinemic-euglycemic clamp studies were performed (Fig. 4C-M). Compared to control and *Ucp2KOKI^Sf1* animals, *Ucp2KO* mice showed significantly lower glucose infusion rate (GIR) to maintain euglycemia (Fig. 4C-E), revealing that UCP2 in VMH neurons is required to regulate insulin sensitivity. Endogenous glucose production (EGP) in *Ucp2KO* mice was higher than controls and selective VMH re-expression of UCP2 in *Ucp2KOKI^Sf1* mice partially restored EGP to the level of controls (Fig. 4F and G). In addition to the liver, whole body glucose utilization (Rd) and rate of glycolysis were significantly lower in *Ucp2KO* mice than controls and *Ucp2KOKI^Sf1* mice (Fig. 4H and I). Consistent with this, 2DG uptake in muscles and BAT were significantly lower in *Ucp2KO* mice compared to controls (Fig. 4J-M), and re-expression of UCP2 in SF1 neurons restored them to control levels (Fig. 4J-M).

To further analyze the role of VMH UCP2 in glucose homeostasis, next, we performed glucose measurements in *Ucp2KI^Sf1* and control mice. No differences in energy metabolism were observed between *Ucp2KI^Sf1* mice and their controls (Fig. S4A-H), including lack of changes in body weight and length (Fig.S4A, B), body fat mass and lean mass (Fig. S4C, D), food intake (Fig. S4E) and energy expenditure in *Ucp2KI^Sf1* (Fig. S4F-H). However, in line with the effect of VMH UCP2 deletion on glucose homeostasis, significant differences in glucose metabolism were observed between *Ucp2KI^Sf1* mice and their controls, whereby *Ucp2KI^Sf1* mice had significantly lower glucose levels during glucose tolerance test (GTT) compared to controls (Fig. 5A). Measurements of circulating insulin levels during GTT showed no significant differences between the experimental groups (Fig. S4I), indicating that the increased glucose tolerance was not due to increased insulin secretion. Analysis of insulin sensitivity by insulin tolerance test (ITT) showed that *Ucp2KI^Sf1* mice were significantly more sensitive to insulin than the controls (Fig. 5B), indicating that overexpression of UCP2 in the VMH enhances insulin sensitivity without changing body weight and composition and insulin secretion. In agreement with this, *Ucp2KI^Sf1* mice had lower gluconeogenic capacity than control mice in a pyruvate tolerance test (PTT; Fig. S4J), which was associated with lower mRNA expression of phosphoenolpyruvate carboxykinase

(PEPCK) in the liver (Fig. S4K). Finally, to determine whether the effect of increased UCP2 expression on glucose metabolism was specific to hyperglycemia, we assessed the effect of glucoprivation, by 2 Deoxyglucose (2DG) injection, in control and *Ucp2KI^{Sf1}* mice. No effect of 2DG on glucose metabolism was observed between the groups (Fig. S4L).

Altogether, these data unmasked that UCP2 in VMH neurons is necessary for appropriate physiological regulation of insulin sensitivity in both muscle and liver.

UCP2-regulated VMH neuronal activation is critical for the control of whole body glucose metabolism

The data above argue for the importance of VMH mitochondrial fission and associated-neuronal activation enabled by UCP2 in the physiological control of systemic glucose metabolism. In the VMH, neuronal subpopulations were identified that are either excited or inhibited by glucose (Chan and Sherwin, 2013). To interrogate whether UCP2 impacts these subpopulations of neurons, we quantified glucose-excited (GE) and glucose-inhibited (GI) neurons in the VMH-SF1 neurons of control and *Ucp2KI^{Sf1}* mice. We performed this measurement in the dorsomedial VMH (dmVMH) since this subdivision showed a larger number of glucose-excited neurons as assessed by c-Fos immunolabeling (Fig. 3M). We observed that in *Ucp2KI^{Sf1}* mice, the GE neuronal subpopulation was significantly larger (10 GE cells/28 total cells/8 mice) than that of control animals (6 GE cells/32 total cells/7 mice; Fig. 5C and E). On the other hand, no differences were found in the GI subpopulation of the dmVMH between transgenic and control animals (control: 2GIcells/32 total cells/7 mice; *Ucp2KI^{Sf1}*: 3GI cells/28 total cells/8 mice; Fig. 5D and F). Furthermore, to determine whether UCP2-mediated increased neuronal excitability to glucose was dependent on K_{ATP} channels, we studied the effect of diazoxide, a K_{ATP} channel opener, on glucose-induced increase of firing rate in dmVMH neurons (Fig. 5G-J). Diazoxide application to excited dmVMH-SF1-GE neurons significantly reduced the firing rates of the majority of these neurons in control (8 cells out of 10 in 5 mice total; Fig. 5G, I and J) and *Ucp2KI^{Sf1}* mice (9 cells out of 11 in 5 mice total; Fig. 5H, I and J). Altogether these observations indicate that systemic glucose control regulated by UCP2 in the VMH is mediated by VMH GE neurons. To test this, we selectively interfered with VMH neuronal activation in response to glucose load in freely moving mice using an inhibiting Designer-Receptors-Exclusively-Activated-by-Designer-Drugs (DREADD) approach (Krashes et al., 2011). We injected inhibitory DREADD (*AAV-hM4Di-mCherry*) into the VMH of control (expressing *cre* in SF1 neurons) and *Ucp2KI^{Sf1}* mice, allowing selective and reversible inactivation of SF1 neurons by application of CNO (0.3 mg/kg BW, i.p.). After virus injection into the VMH, locally restricted expression of *the virus* was specified by *mCherry* fluorescence (Fig. 6A, B, Fig. S5). Thirty minutes after CNO-driven activation of the inhibitory DREADD, glucose was injected and circulating glucose levels measured. Compared to the vehicle-injected mice 30 minutes prior glucose administration, control and *Ucp2KI^{Sf1}* mice injected first with CNO and then with glucose (Fig. 6C and D) displayed a significant increase in circulating glucose levels that were similar between these two groups (Fig. 6C and D). Finally, to determine whether UCP2 overexpression-induced increased neuronal excitability to glucose was selective of the VMH, we assessed the effect of UCP2 overexpression in cortical neuronal excitability after a glucose load. First, no difference in cortical cfos staining was observed

between control and $Ucp2KI^{Sf1}$ mice injected either with saline or glucose (Fig. S6A and B). Furthermore, when $Ucp2KI^{flox/flox}$ mice were injected either with AAV-GFP or AAV-cre-GFP in the cortex (medial parietal associational cortex, MPtA) to generate control and $Ucp2KI^{MPtA}$ mice, respectively, glucose load did not alter cfos immunoreactivity between these 2 experimental groups or compared to saline-treated groups (Fig.S6C and D), suggesting that UCP2-induced increased neuronal excitability is specific of VMH glucose-sensing neurons.

Altogether these observations provide direct evidence that inhibition of VMH neurons results in impaired glucose uptake in the periphery in response to a glucose load and suggest that UCP2-dependent mitochondrial fission in GE neurons mediates VMH control of systemic glucose metabolism.

Discussion

Our studies show that glucose-induced VMH mitochondrial fission mediated by DRP1 activation and increased neuronal activation, are UCP2-dependent and necessary for the proper control of peripheral glucose metabolism. Whole body UCP2 knockout ($Ucp2KO$) mice, in which glucose did not induce these cellular processes, showed glucose intolerance due to reduced insulin sensitivity in peripheral organs. On the other hand, selective re-expression of UCP2 in SF1 neurons ($Ucp2KOKI^{Sf1}$) restored mitochondrial dynamics, DRP1 activation, and neuronal activity after increased glucose levels and re-established insulin sensitivity in peripheral organs. Consistent with these data, mice with selective overexpression of UCP2 ($Ucp2KI^{Sf1}$) in SF1 neurons showed enhanced mitochondrial fission, increased DRP1 activation that resulted in increased VMH neuronal activity and improved glucose metabolism. Furthermore, when SF1 neurons were selectively inactivated by DREADD, glucose metabolism worsened in both $Ucp2KI^{Sf1}$ and control mice. Altogether, our data unmasked that UCP2 in SF1 neurons, by affecting mitochondrial dynamics and neuronal activity, is crucial in the regulation of glucose metabolism of peripheral tissues.

The hypothalamus plays a critical role in the homeostatic control of blood glucose levels by altering glucose production in the liver, glucose utilization in peripheral tissues (Grayson et al., 2013) and by controlling pancreatic secretion of hormones, including insulin (Kim et al., 2014). Within the hypothalamus, the ventromedial nucleus (VMH) has been shown to play a critical role in controlling glucose homeostasis via its glucose sensing neurons. Neurons in the VMH express the inner mitochondrial protein, uncoupling protein 2 (UCP2; Horvath et al., 1999; Richard et al., 1998), of which function in these cells has not been defined.

Previous data from our laboratory have shown that UCP2 expression in arcuate neurons induces mitochondrial changes (Andrews et al., 2008; Coppola et al., 2007). The present study shows that UCP2 in VMH neurons also induces mitochondrial changes i.e., increase in mitochondrial density and reduction in mitochondrial size, suggesting that UCP2 expression is associated with a mitochondrial fission process. In support of this, DRP1 activation, a major component of the mitochondrial fission process (Kasahara and Scorrano, 2014), was increased in the VMH after glucose administration. UCP2 control of DRP1-dependent

fission in VMH neurons is critical for whole body glucose regulation since suppression of UCP2 expression in these neurons induced a significant deleterious effect on glucose metabolism, while VMH UCP2 overexpression significantly improved peripheral glucose metabolism. In accordance with these data, a study from Carneiro and collaborators has shown that intracarotid glucose infusion in rats increases mitochondrial number in the VMH neurons, and suppression of this increase attenuates glucose sensing in the VMH neurons (Carneiro et al., 2012).

Our data show that the activation of VMH neurons, and specifically neurons located in the dorsomedial VMH (dmVMH), by UCP2 enhances insulin sensitivity in peripheral tissues. In line with this, intra-VMH injection of leptin, which activates dmVMH SF1 neurons co-expressing leptin receptors (Dhillon et al., 2006), enhances insulin sensitivity in both muscles and liver. This occurs through a melanocortin receptor-dependent pathway in the muscle and a melanocortin–independent pathway in the liver (Toda et al., 2013; Toda et al., 2009). In addition, orexin-induced activation of VMH neurons also increases glucose uptake in the muscle (Shiuchi et al., 2009). This activation occurs via the sympathetic nervous system (SNS; Shiuchi et al., 2009). On the other hand, regulation of hepatic glucose production by hypothalamic nutrient sensing has been shown to be mediated by the vagus nerve (Lam et al., 2005a; Lam et al., 2005b). Therefore, it is reasonable to suggest that UCP2-induced VMH activation affects insulin sensitivity in peripheral tissues via the autonomic nervous system. Indeed, SF1-positive fibers have been shown to project to the autonomic centers, such as the hypothalamic paraventricular (PVN) and dorsomedial nuclei (DMH), the periaqueductal gray (PAG), the rostral ventrolateral medulla (RVLM) and the nucleus of the solitary tract (NTS) (Lindberg et al., 2013).

We found that UCP2-induced mitochondrial fission in the VMH affects GE neurons while it does not alter GI neurons. These data suggest that this mechanism is specific for appropriate neuronal responsiveness to hyperglycemia. In support of this, in our study, glucoprivation, induced by 2DG, in *Ucp2KI^Sf1* mice did not significantly alter glucose metabolism compared to control mice. Furthermore, hypoglycemia and hypoglycemia-induced counter regulatory responses have been associated with changes in the activity of GI neurons (Fioramonti et al., 2011).

In summary, our studies revealed a physiological role for UCP2 in the ventromedial SF1 neurons of the hypothalamus in the regulation of glucose homeostasis. This mechanism by regulating mitochondrial dynamics and the excitability of VMH glucose-sensing neurons allows the appropriate response to increased glucose levels resulting in the enhancement in insulin sensitivity in peripheral organs.

EXPERIMENTAL PROCEDURES

Animals

All animal work was approved by the Yale University Institutional Animal Care and Use Committee. Mice were housed at 22°C–24°C with a 12 hr light/12 hr dark cycle with standard chow (Harlan Teklad no. 2018, 18% calories from fat) and water provided ad libitum. All mice studied were on a mixed background (129SvEv, FVB and C57BL/6J).

Generation of mice conditionally expressing UCP2

A construct was engineered in which expression of murine Ucp2 cDNA is controlled by the CAGGS promoter upon Cre-mediated deletion of a transcriptional STOP cassette. A Ucp2 cDNA was introduced into the Asc I site of a STOP-EGFP-ROSA-CAGGS targeting vector (Sasaki et al., 2006). This construct was then used to create a knockin at the ROSA locus by homologous recombination in B6;129F1 ES cells, and targeted clones were injected into C57Bl/6 blastocysts to generate mutant mice (*Ucp2KI^{flox/flox}* mice).

To generate Sf1 neurons-specific overexpression of Ucp2 gene, *Ucp2KI^{flox/flox}* mice were crossed with *Sf1-cre* mice, which express cre recombinase in a subset group of neurons of the VMH (Dhillon et al., 2006). *Sf1-cre* mice were purchased from the Jackson laboratory (STOCK Tg(Nr5a1-cre)7Lowl/J; Bar Harbor, ME). *UCP2KI^{fl/+}-Sf1 cre* mice were crossed to produce control mice (*Ucp2KI^{fl/fl}*-cre negative or *Ucp2KI^{+/+}*-cre positive mice) and *Ucp2KI^{Sf1}*.

Ucp2KI^{fl/fl} mice were also crossed with whole body UCP2 knockout mice (*Ucp2KO)* to produce *Ucp2^{-/+}-KI^{fl/+}* mice. These mice were then crossed with *Sf1-cre* mice to generate *Ucp2^{-/+}-KI^{fl/+}* -cre positive mice. Crossing between these mice were then arranged to generate *Ucp2^{-/-}-KI^{+/+}* mice (*Ucp2KO* mice), *Ucp2^{-/-}-KI^{Sf1}* (*Ucp2KOKI^{Sf1}*) mice, and controls (*Ucp2^{+/+}-Ucp2KI^{fl/+}*either cre positive or negative and *Ucp2^{-/+}-KI^{fl/+}* either cre positive or negative.

Indirect calorimetry system and body composition

Animals were acclimated in metabolic chambers (TSE System-Core Metabolic Phenotyping Center, Yale University) for 3 days before the start of the recordings. Mice were continuously recorded for 2 days, with the following measurements taken every 30 min: food intake, locomotor activity (in the xy- and z-axes), and gas exchange (O_2 and CO_2; The TSE LabMaster System). Energy expenditure was calculated according to the manufacturer's guidelines (PhenoMaster Software, TSE System). The respiratory quotient was estimated by calculating the ratio of CO_2 production to O_2 consumption. Values were adjusted by body weight to the power of 0.75 (kg−0.75) where mentioned. Body composition was measured in vivo by MRI (EchoMRI; Echo Medical Systems, Houston, TX).

Measurement of circulating hormones

Serum from blood samples was obtained by centrifugation at 3,000 rpm for 15 min, and each circulating hormone was determined using a commercially available ELISA kit as follows: insulin (Rat/Mouse Insulin ELISA kit, EZRMI-13K; Millipore) and glucagon (Glucagon Qkit, DGCG0; R&D Systems). All procedures were performed by following the manufacturer's protocol.

Glucose, insulin and pyruvate tolerance tests and 2DG test

Glucose tolerance tests were performed in 16h fasted animals as previously reported (Kim et al., 2014; Long et al., 2014). Each animal received an ip injection of 2g/kg BW glucose

(DeltaSelect, Germany) in sterile saline. Blood glucose and insulin levels were measured after 15, 30, 60 and 120 minutes.

Insulin tolerance test was performed in *ad libitum* fed mice (Kim et al., 2014). Each animal received an ip injection of insulin, 1U/kg (Humulin R; Eli Lilly, Indianapolis, IN). Blood glucose levels were then measured at 15, 30, 60, and 120 min after insulin injection.

Pyruvate tolerance test (PTT) was performed in 16h fasted animals. Animals received an ip injection of 2g/kg BW sodium pyruvate (Sigma-Aldrich, St. Louis, MO, Cat#P5280). Blood glucose levels were then monitored at 15, 30, 60, and 120 min after the injection.

2Deoxyglucose (2DG) test was performed by ip injection of 200mg/kg BW 2DG (Sigma-Aldrich, St. Louis, MO). Blood glucose levels were then monitored at 15, 30, 60, and 120 min after the injection.

Surgical procedure for clamp studies

For the hyperinsulinemic-euglycemic clamp, polyethylene catheters were inserted into the right carotid arteries and jugular veins of mice after they were anesthetized with ketamine (100 mg/kg body mass) and xylazine (10 mg/kg). Animals were individually housed after surgery, and lines were flushed daily with 50 μl heparinized saline for the 3-5 days recovery period.

Hyperinsulinemic-euglycemic clamp and measurement of associated 2-[^{14}C]Deoxy-D-glucose (2DG) uptake

The hyperinsulinemic-euglycemic clamp protocol was measured as described previously (Ayala et al., 2006; Kim et al., 2014; Long et al., 2014; Toda et al., 2013), initiated in conscious and unrestrained mice after the fasting for four hours. The 90-min basal period (t = –90 to 0 min) was followed by a 115-min clamp period (t = 0 to 115 min) (Figure 3F). A priming dose of [3-^{3}H]glucose (5 μCi) (Perkin Elmer, Waltham, MA) was administered at t = –90 min and was followed by infusion of the tracer at a rate of 0.05 μCi/min for 1.5 h. For assessment of Ra during the basal period, blood samples (50 μl) were collected at t = –15 and –5 min.

The clamp period was initiated at t = 0 min by primed and continuous infusion of human insulin (bolus of 8 mU/kg followed by a rate of 1.25 mU kg^{-1} min^{-1} for female control, *Ucp2KO* and *Ucp2KOKI^{Sf1}* mice) (Humulin R; Eli Lilly, Indianapolis, IN). The rate of [3-^{3}H]glucose infusion was increased to 0.1 μCi/min for the remainder of the experiment in order to minimize changes in specific activity relative to the equilibration period. Blood was collected every 5 to 10 min from the carotid artery catheter and blood glucose was monitored (One Touch Ultra; Lifescan, Johnson & Johnson). Glucose (30%) was infused at a variable rate via the jugular vein catheter in order to maintain blood glucose levels at 110 to 130 mg/dl. Withdrawn erythrocytes were suspended in sterile 0.9% saline and returned to each animal.

Tissue 2DG uptake was measured as described previously (Toda et al., 2013). For assessment of 2DG uptake, mice were infused 2-[^{14}C]DG (10 μCi) at t = 70 min, and blood

samples (50 μl) were collected at t = 75, 85, 95, 105, and 115 min. Immediately after collection of the final blood sample (t = 0 min or 115 min), mice were euthanatized, and soleus, Gastro-R (red portion of gastrocnemius), Gastro-W (white portion of gastrocnemius), BAT (interscapular brown adipose tissue), heart, spleen, EWAT (epididymal while adipose tissue), brain (cortex) and the liver were rapidly dissected. Gastro-R was dissected from the inner surface of gastrocnemius attaching soleus muscle, while Gastro-W was dissected from the outer surface of the muscle. Mice were euthanatized, and soleus, Rd (Rate of disappearance), which reflects whole-body glucose utilization, Ra (Rate of appearance), which reflects EGP, and the rates of whole-body glycolysis and glycogen synthesis were determined as described previously (Ayala et al., 2006).

c-fos immunostaining

After overnight fasting, mice were injected with either saline (same volume than glucose) or glucose (2g/kg, ip) and after 1 h from the injection they were perfused with saline following 4% PFA transcardially. Serial sections of the entire VMH were collected 150μm apart and incubated with the rabbit anti-c-fos antibody (Santacruz, 1:2000) and the mouse anti-mCherry antibody (Life Technologies Corporation, Grand Island, NY, USA, 1:3000) in PB containing 4% normal goat serum, 1% glycine and 0.2% Triton X-100 for 24 hr at room temperature. After several washes with PB, sections were incubated in the secondary antibodies (biotinylated goat anti-rabbit IgG; 1:250 in PB; Vector Laboratories and goat anti-mouse fluor 633; 1:250 in PB; Life Technologies) for 2 hr at room temperature, then rinsed in PB three times 10 min each time, and incubated for 2 hr at room temperature with Alexa Fluor® 594 streptavidin (Life Technologies, 1:2000 in PB). Sections were mounted on glass slide with vectashield (Vector lab) and analyzed with fluorescent microscope.

DHE administration

ROS levels in dmVMH SF1 neurons were measured by injecting dihydroethidium (DHE, 1mg/ml; Invitrogen) through tail vain (Andrews et al., 2008). Two hours after the DHE injection, glucose (2g/kg BW) was injected and one hour after the glucose injection, mice were anesthetized and transcardially perfused with 0.9% saline with heparin followed by fixative (4% paraformaldehyde, 15% picric acid, 0.1% glutaraldehyde in PBS). Brains were collected and post-fixed overnight before coronal sections were taken at every 50 μm. Sections were washed and and blocking with 2% normal horse serum, sections were incubated with primary antibodies; anti-chicken eGFP antibody (1:1000, Life Technologies) 4 C° overnight protected from the light. Sections were then washed and incubated with secondary antibody (goat antichicken Alexa-fluor 488; 1:200 for 60 minutes at RT). Sections were then mounted with VectaShield antifade (Vector Laboratories). Fluorescent images of five to seven brain sections were captured with confocal microscope and analyzed by imaging Software (Image J).

Electron Microscopy analysis

Saline and glucose injected (2g/kg ip, 1hr) mice were anesthetized and transcardially perfused with 0.9% saline followed by fixative (4% paraformaldehyde, 15% picric acid, 0.1% glutaraldehyde in 0.1 M PB. Brains were stained with nickeldiaminobenzidine

(NicoDAB) by using anti-GFP antibody (1:5000). After several washes with PB, sections were incubated in the secondary antibody (biotinylated goat antirabbit IgG; 1:250 in PB; Vector Laboratories) for 2 hr at room temperature, then rinsed in PB three times 10 min each time, and incubated for 2 hr at room temperature with avidin–biotin–peroxidase (ABC; 1:250 in PB; ABC Elite kit, Vector Laboratories). The immunoreaction was visualized with 3,3-diaminobenzidine (DAB).

Sections were then osmicated (1% osmium tetroxide) for 30 min, dehydrated through increasing ethanol concentrations (using 1% uranyl acetate in the 70% ethanol for 30 min), and flat-embedded in araldite between liquid release-coated slides (Electron Microscopy Sciences, Fort Washington, PA). After capsule embedding, blocks of the dmVMH were trimmed. Ribbons of serial ultrathin sections were collected on Formvar-coated single slot grids and examined using a Philips CM-10 electron microscope. Mitochondria were counted blindly from randomly selected sections, and Image J software was used to normalize cytoplasmic area so that mitochondrial density is expressed as number of mitochondria per square micrometers of cytosol.

Western blot analysis

Protein lysates from hypothalamic VMH punches were prepared by modified RIPA buffer (50 mM Tris-HCl, pH 7.5, 150 mM NaCl, 1mM EDTA, 1% TritonX-100, 0.1% SDS, 1 mM phenylmethylsulfonyl fluoride) supplemented with protease inhibitor cocktail (Roche, Cat# 11 836 170 001) and Halt Phosphatase Inhibitor (product # 78420, Thermo Fisher Scientific) on ice for 30 minutes followed by centrifugation at 14,000 rpm for 15 minutes. Protein concentrations were measured using the BCA kit (Thermo scientific, Cat# 23228 and 1859078). Proteins was resolved on 10% SDS-PAGE and transferred to PVDF membrane (Millipore, Cat# IPVH 15150). Membranes were blocked with 5% dry milk in TBS (50mM Tris-HCl, pH 7.5, 150mM NaCl) for 1 hour, followed by overnight incubation at 4°C with primary antibodies such as anti-phospho-DRP1 (Ser616) antibody (Cell signaling, Cat# 4494) and anti-Drp1 antibody (BD Biosciences, Cat# 611112). Membranes were washed 3 times with TBST (TBS including 0.05% Tween 20) and then incubated with either anti-rabbit IgG conjugated to horseradish peroxidase (HRP) for anti-p-Drp1 antibody (Santa Cruz Biotechnology, Cat# sc-2004) or anti-mouse IgG-HRP (Santa Cruz Biotechnology, Cat# sc-2005) for anti-Drp1 antibody for 1 hour and developed by ECL kit (Thermo scientific, Cat# 32016). Membranes were reused to detect β-actin (Sigma, Cat# A5441) after stripping with Restore™ PLUS western blot stripping buffer (Thermo scientific, Cat#46430).

Real-time PCR

Total RNA from liver was extracted from the animals using Trizol solution (Invitrogen). Phosphoenolpyruvate carboxykinase (PEPCK) mRNA levels in the liver were measured by real-time PCR. A High Capacity cDNA Reverse transcription Kit (Applied Biosystems) was used for the reverse transcription. Real-time PCR (LightCycler 480; Roche) was performed with diluted cDNAs in a 20-μl reaction volume in triplicates. Primers used for this study are as follows: Mm 01247058_m1 for PEPCK, Mm99999915_g1 for DAPDH and Mm0.928990_g1 for 18S rRNA (Applied Biosystems). The calculations of average Cp

values, SDs, and resulting expression ratios for each target gene were based on the Roche LightCycler 480 software.

Electrophysiology

Seven to eight-weeks-old mice were used and the hypothalamic slices were prepared as described previously (Liu et al., 2011). Briefly, after mice were anaesthetized with isoflurane and decapitated, the brains were rapidly removed and immersed in cold (4°C) oxygenated high-sucrose solution containing (mM): sucrose 220, KCl 2.5, NaH_2PO_4 1.23, $NaHCO_3$ 26, $CaCl_2$ 1, $MgCl_2$ 6 and glucose 10, pH 7.3 with NaOH. After being trimmed to a small tissue block containing the hypothalamus, coronal slices (300 μm thick) were cut on a vibratome and maintained in a holding chamber with artificial cerebrospinal fluid (ACSF, bubbled with 5% CO_2 and 95% O_2) containing (in mM): NaCl 124, KCl 3, $CaCl_2$ 2, $MgCl_2$ 2, NaH_2PO_4 1.23, $NaHCO_3$ 25, glucose 2.5, pH 7.4 with NaOH. After a one-hour recovery period, slices were transferred to a recording chamber and were constantly perfused with ACSF (33°C) at a rate of 2 ml min–1.

Perforated patch recording was performed in SF1-GFP neurons of dmVMH under voltage- and current clamp. The micropipettes were made of borosilicate glass (World Precision Instruments) with a Sutter micropipette puller (P-97) and back filled with a pipette solution containing (mM): potassium methanesulfonate 135, MgCl2 2, Hepes 10, EGTA 0.2, Mg-ATP 2, Na_2-GTP 0.3, Na2-phosphocreatin 10 and amphotericin B (Sigma, final concentration 50 μg/ml), pH 7.3 with KOH. Both input resistance and series resistance were monitored throughout the experiments and the former was partially compensated. Only those recordings with stable series resistance and input resistance were accepted. The membrane and spontaneous action potential were recorded in SF1 neurons under current clamp. We recorded action potential firing for 4-8min at a glucose concentration of 2.5mM. When firing was stable, glucose concentration was changed to 0.2mM for 4 minutes before to return to 2.5mM glucose for 6 minutes.

At the end of the perforated patch recordings, the membrane of every cell was ruptured and whole cell patch recording measured to check current-voltage relationship. All data were sampled at 3–10 kHz, filtered at 1–3 kHz and analyzed with an Apple Macintosh computer using AxoGraph × (AxoGraph Scientific). Statistics and plotting were performed with KaleidaGraph (Synergy software) and Igor Pro (WaveMetrics).

The average firing rate was calculated in the last 2 minutes of each glucose concentrations. Cells with 30% change in firing rate were considered either GE or GI neurons.

To check the involvement of the K_{ATP} channel, perforated patch recording was performed in SF1-GFP neurons as reported above changing glucose concentration from 2.5mM to 0.2mM. Glucose concentration was returned to 2.5mM for 5-8 minutes only in cells that responded to decreased glucose concentration by reducing their firing rates (GE neurons). At this point, diazoxide, a K_{ATP} channel opener (Sigma, final concentration 300 μM) was added to the solution. The average firing rate was calculated in the last 3 minutes of 2.5mM glucose alone and of 2.5mM glucose+diazoxide. Data were compared using unpaired t-tests,

with P <0.05 considered as a K_{ATP} channel-mediated GE neuron. All the experiments were performed blindly to the electrophysiologist.

Stereotaxic AAV-DREADD virus injection

The AAV5/hSyn-DIO-hM4D-mCherry virus (University North Carolina VectorCore) was injected bilaterally into the VMH as previously described (Franklin KBJ; Krashes et al., 2011). Ten-12 weeks old *Sf1-cre* male mice were anesthetized with 100mg/kg ketamine and 10mg/kg xylazine (i.p.) and placed in stereotaxic apparatus. A guide cannula with dummy cannula (Plastics one, Roanoke, VA) was inserted into the VMH according to the atlas of Franklin and Paxinos (Franklin KBJ) (From Bregma, anteroposterior: −1.4mm; mediolateral: 0.4mm; dorsoventral: −5.8mm). 0.5 μl of AAV virus (1.0×10^{12} VG/ml) was administered using an injector (Plastics one) connected with a Hamilton syringe at a rate of 33.3 nL/minute. Five min following the injection (to allow for adequate dispersal and absorption of the virus), the same volume of the virus was injected into the contralateral VMH. Animals were administered an analgesic subcutaneously (4mg/kg Meloxicam SR™ LAB, Zoopharm, Laramie, WY) and given 1 week recovery before a GTT was performed. For the GTT, overnight fasted mice were injected i.p. with Clozapine-N-oxide (CNO, 0.3mg/kg, Sigma-Aldrich). Thirty minutes after CNO administration, 2g/kg BW of glucose (DeltaSelect, Germany) in sterile saline was i.p. injected and blood glucose levels were measured after 15, 30, 60 and 120 minutes.

Stereotaxic viral injections in the cortex

The AAV2-GFP and AAV2-Cre-GFP virus (VECTOR BIOLABS) was injected bilaterally into the medial parietal association cortex (MPtA). Eight weeks old *Ucp2KI^{flox/flox}* male mice (n=3 per group) were anesthetized with 100mg/kg ketamine and 10mg/kg xylazine (i.p.) and placed in stereotaxic apparatus. A guide cannula with dummy cannula (Plastics one, Roanoke, VA) was inserted into the MPtA according to the atlas of Franklin and Paxinos (Franklin KBJ) (From Bregma, anteroposterior: −1.4mm; mediolateral: −1mm; dorsoventral: −1mm) and 0.5 μl of either AAV2-GFP virus (1.0×10^{12} VG/ml) or AAV2-Cre-GFP virus (1.0×10^{12} VG/ml) was administered using an injector (Plastics one) connected with a Hamilton syringe at a rate of 33.3 nL/minute. After 10 days, mice were fasted overnight and injected the morning after with either saline (same volume than glucose) or glucose (2g/kg, ip) and transcardially perfused (as described above) one hour from the injection. Brain sections were then stained for cfos and analyzed as described above.

Statistical analysis

All analyses were performed blinded to the individual performing the experiment and analysis. Two-way ANOVA was used to determine the effect of the genotype and diet with the Prism 4.0 software (GraphPad Software, San Diego, CA). For repeated-measures analysis, ANOVA was used when values over different times were analyzed. Significant effects were evaluated followed with Fisher's protected least significant difference post hoc test with Tukey or Bonferroni's correction. When only two groups were analyzed, statistical

significance was determined by unpaired Student t-test. A value of $P < 0.05$ was considered statistically significant. All data are shown as means ± SEM.

Supplementary Material

Refer to Web version on PubMed Central for supplementary material.

ACKNOWLEDGMENTS

Reference

Andrews Z, Liu Z-W, Walllingford N, Erion D, Borok E, Friedman J, Tschöp M, Shanabrough M, Cline G, Shulman G, et al. UCP2 mediates ghrelin's action on NPY/AgRP neurons by lowering free radicals. Nature. 2008; 454:846–851. [PubMed: 18668043]

Ayala JE, Bracy DP, McGuinness OP, Wasserman DH. Considerations in the design of hyperinsulinemic-euglycemic clamps in the conscious mouse. Diabetes. 2006; 55:390–397. [PubMed: 16443772]

Borg WP, During MJ, Sherwin RS, Borg MA, Brines ML, Shulman GI. Ventromedial hypothalamic lesions in rats suppress counterregulatory responses to hypoglycemia. J Clin Invest. 1994; 93:1677–1682. [PubMed: 8163668]

Carneiro L, Allard C, Guissard C, Fioramonti X, Tourrel-Cuzin C, Bailbe D, Barreau C, Offer G, Nedelec E, Salin B, et al. Importance of mitochondrial dynamin-related protein 1 in hypothalamic glucose sensitivity in rats. Antioxidants & redox signaling. 2012; 17:433–444. [PubMed: 22229526]

Chan O, Sherwin R. Influence of VMH fuel sensing on hypoglycemic responses. Trends in endocrinology and metabolism: TEM. 2013; 24:616–624. [PubMed: 24063974]

Coppola A, Liu ZW, Andrews ZB, Paradis E, Roy MC, Friedman JM, Ricquier D, Richard D, Horvath TL, Gao XB, et al. A central thermogenic-like mechanism in feeding regulation: an interplay between arcuate nucleus T3 and UCP2. Cell Metab. 2007; 5:21–33. [PubMed: 17189204]

Dhillon H, Zigman J, Ye C, Lee C, McGovern R, Tang V, Kenny C, Christiansen L, White R, Edelstein E, et al. Leptin directly activates SF1 neurons in the VMH, and this action by leptin is required for normal body-weight homeostasis. Neuron. 2006; 49:191–203. [PubMed: 16423694]

Diano S, Horvath T. Mitochondrial uncoupling protein 2 (UCP2) in glucose and lipid metabolism. Trends in molecular medicine. 2012; 18:52–58. [PubMed: 21917523]

Dietrich M, Horvath T. Hypothalamic control of energy balance: insights into the role of synaptic plasticity. Trends Neurosci. 2013; 36:65–73. [PubMed: 23318157]

Fioramonti X, Song Z, Vazirani RP, Beuve A, Routh VH. Hypothalamic nitric oxide in hypoglycemia detection and counterregulation: a two-edged sword. Antioxidants & redox signaling. 2011; 14:505–517. [PubMed: 20518706]

Franklin KBJ, PG. The Mouse Brain in Stereotaxic Coordinates. 3rd. Academic Press; San Diego, CA: 2007.

Grayson BE, Seeley RJ, Sandoval DA. Wired on sugar: the role of the CNS in the regulation of glucose homeostasis. Nature reviews Neuroscience. 2013; 14:24–37. [PubMed: 23232606]

Horvath TL, Warden CH, Hajos M, Lombardi A, Goglia F, Diano S. Brain uncoupling protein 2: uncoupled neuronal mitochondria predict thermal synapses in homeostatic centers. J Neurosci. 1999; 19:10417–10427. [PubMed: 10575039]

Kasahara A, Scorrano L. Mitochondria: from cell death executioners to regulators of cell differentiation. Trends Cell Biol. 2014; 24:761–770. [PubMed: 25189346]

Kim JD, Toda C, D'Agostino G, Zeiss CJ, DiLeone RJ, Elsworth JD, Kibbey RG, Chan O, Harvey BK, Richie CT, et al. Hypothalamic prolyl endopeptidase (PREP) regulates pancreatic insulin and

glucagon secretion in mice. Proc Natl Acad Sci U S A. 2014; 111:11876–11881. [PubMed: 25071172]

Krashes M, Koda S, Ye C, Rogan S, Adams A, Cusher D, Maratos-Flier E, Roth B, Lowell B. Rapid, reversible activation of AgRP neurons drives feeding behavior in mice. The Journal of clinical investigation. 2011; 121:1424–1428. [PubMed: 21364278]

Lam TK, Gutierrez-Juarez R, Pocai A, Rossetti L. Regulation of blood glucose by hypothalamic pyruvate metabolism. Science. 2005a; 309:943–947. [PubMed: 16081739]

Lam TK, Pocai A, Gutierrez-Juarez R, Obici S, Bryan J, Aguilar-Bryan L, Schwartz GJ, Rossetti L. Hypothalamic sensing of circulating fatty acids is required for glucose homeostasis. Nat Med. 2005b; 11:320–327. [PubMed: 15735652]

Lindberg D, Chen P, Li C. Conditional viral tracing reveals that steroidogenic factor 1-positive neurons of the dorsomedial subdivision of the ventromedial hypothalamus project to autonomic centers of the hypothalamus and hindbrain. J Comp Neurol. 2013; 521:3167–3190. [PubMed: 23696474]

Liu ZW, Gan G, Suyama S, Gao XB. Intracellular energy status regulates activity in hypocretin/orexin neurones: a link between energy and behavioural states. J Physiol. 2011; 589:4157–4166. [PubMed: 21727218]

Long L, Toda C, Jeong JK, Horvath TL, Diano S. PPARgamma ablation sensitizes proopiomelanocortin neurons to leptin during high-fat feeding. J Clin Invest. 2014; 124:4017–4027. [PubMed: 25083994]

Morton G, Schwartz M. Leptin and the central nervous system control of glucose metabolism. Physiological reviews. 2011; 91:389–411. [PubMed: 21527729]

Richard D, Rivest R, Huang Q, Bouillaud F, Sanchis D, Champigny O, Ricquier D. Distribution of the uncoupling protein 2 mRNA in the mouse brain. J Comp Neurol. 1998; 397:549–560. [PubMed: 9699915]

Sandoval DA, Obici S, Seeley RJ. Targeting the CNS to treat type 2 diabetes. Nature reviews Drug discovery. 2009; 8:386–398. [PubMed: 19404312]

Sasaki Y, Derudder E, Hobeika E, Pelanda R, Reth M, Rajewsky K, Schmidt-Supprian M. Canonical NF-kappaB activity, dispensable for B cell development, replaces BAFF-receptor signals and promotes B cell proliferation upon activation. Immunity. 2006; 24:729–739. [PubMed: 16782029]

Shiuchi T, Haque M, Okamoto S, Inoue T, Kageyama H, Lee S, Toda C, Suzuki A, Bachman E, Kim Y-B, et al. Hypothalamic orexin stimulates feeding-associated glucose utilization in skeletal muscle via sympathetic nervous system. Cell metabolism. 2009; 10:466–480. [PubMed: 19945404]

Toda C, Shiuchi T, Kageyama H, Okamoto S, Coutinho EA, Sato T, Okamatsu-Ogura Y, Yokota S, Takagi K, Tang L, et al. Extracellular signal-regulated kinase in the ventromedial hypothalamus mediates leptin-induced glucose uptake in red-type skeletal muscle. Diabetes. 2013; 62:2295–2307. [PubMed: 23530005]

Toda C, Shiuchi T, Lee S, Yamato-Esaki M, Fujino Y, Suzuki A, Okamoto S, Minokoshi Y. Distinct effects of leptin and a melanocortin receptor agonist injected into medial hypothalamic nuclei on glucose uptake in peripheral tissues. Diabetes. 2009; 58:2757–2765. [PubMed: 19752162]
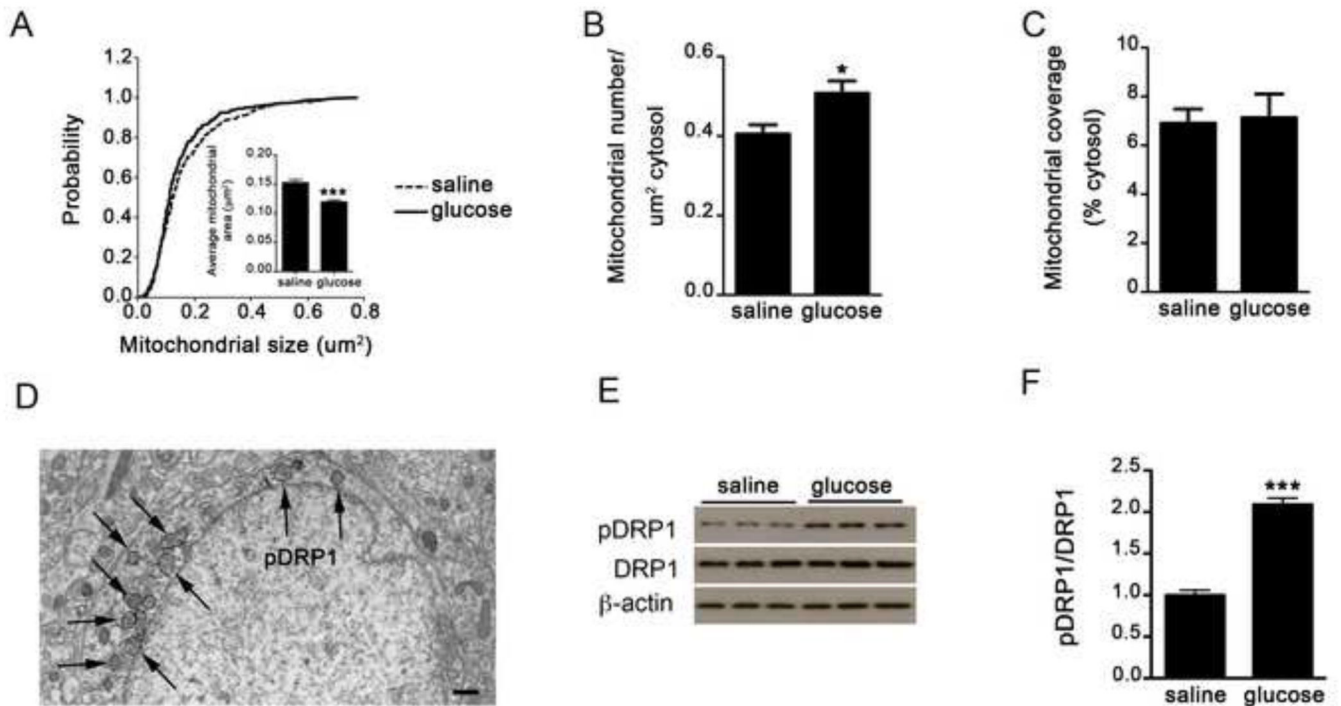
Figure 1. Glucose induces mitochondrial fission and DRP1 activation

A-C: Cumulative probability distribution of cross-sectional mitochondria area (A), Mitochondria density (B) and mitochondria coverage (C) in SF1 neurons from control mice injected with either saline or glucose (ip, 2g/kg BW). n (control mice with ip saline) = 485 mitochondria/22 cells/4 mice; n (control mice with ip glucose) = 445 mitochondria/18 cells/3 mice.

D: Representative electron micrograph showing phosphorylated DRP1 (pDRP1) staining (arrows) associated with mitochondrial membrane in a VMH neuron.

E-F: Representative Western blot (E) and densitometry results (F) for phosphorylation of DRP1 at Ser616 (pDRP1), total DRP1 (DRP1) and β-actin in VMH samples from control mice 30 minutes after saline (n=5) or glucose injection (n=5).

All data represent the mean±SEM. Bar scale in panel D represents 500 nm. *=P<0.05; ***=P<0.001.
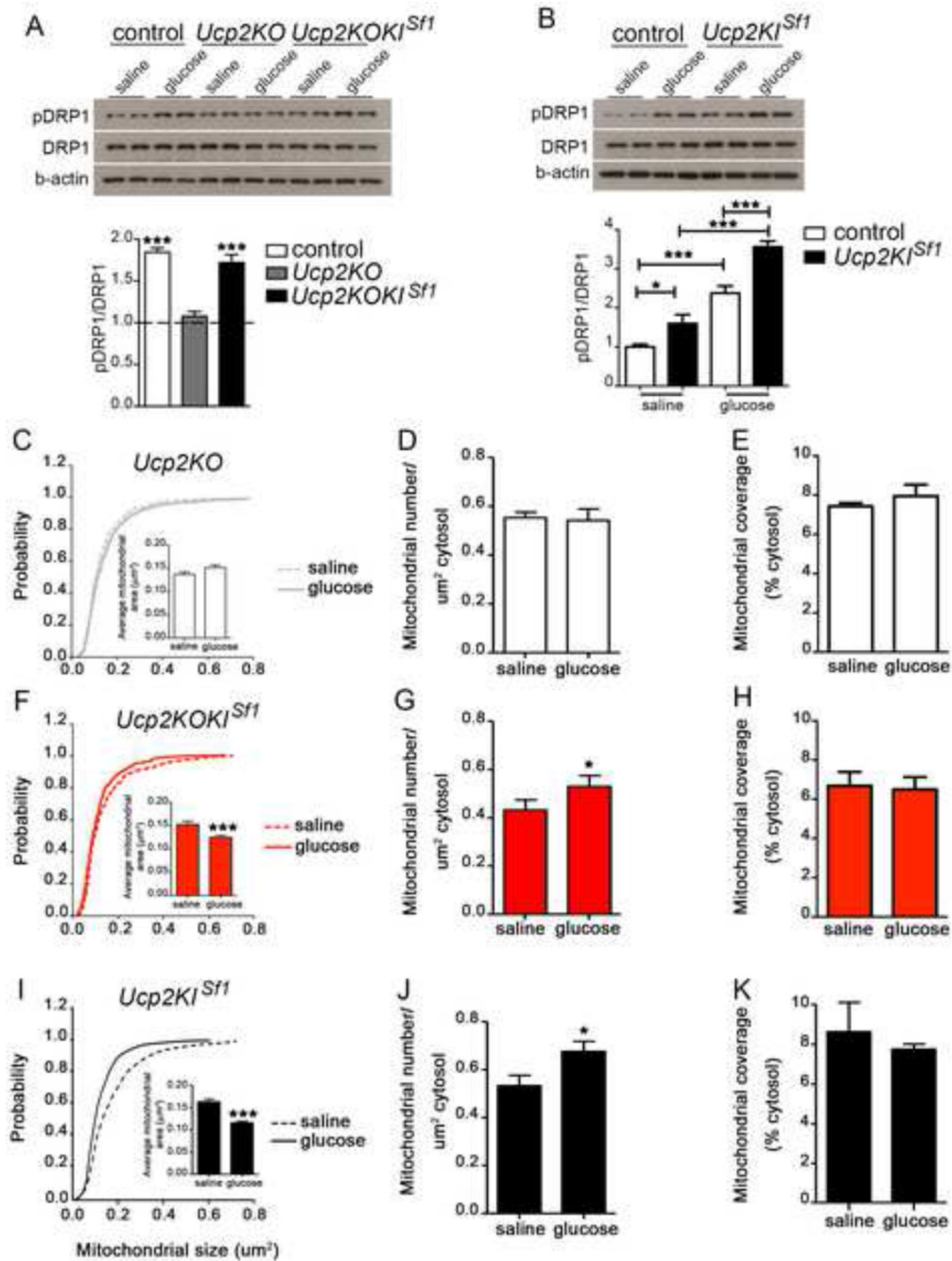
Figure 2. UCP2 in SF1 neurons regulates mitochondrial fission, DRP1 activation and neuronal activation in response to glucose

A: Representative Western blot and densitometry results for phosphorylation of DRP1 at Ser616 (pDRP1), total DRP1 (DRP1) and β-actin in VMH samples from control, *Ucp2KO* and *Ucp2KOKI^Sf1* mice 30 minutes after saline (n=4 per group) or glucose injection (n=4 per group). Dotted line indicates pDRP1/DRP1 levels for each experimental group 30 minutes after saline administration. Note that no difference in pDRP1/DRP1 ratio was observed between groups after saline injection.

B: Representative Western blot image and densitometry for phosphorylation of DRP1 at Ser616 (pDRP1), total DRP1 (DRP1) and β-actin in VMH samples from control, and *Ucp2KI^{Sf1}* mice 30 minutes after either saline (n=4 per group) or glucose injection (n=4 per group). Densitometry results of the Western blots showing pDRP1/DRP1 ratio in the experimental groups after glucose administration. Note that pDRP1/DRP1 ratio after saline administration is significantly greater in *Ucp2KI^{Sf1}* mice compared to controls.

C-E: Cumulative probability distribution of cross-sectional mitochondria area (C), Mitochondria density (D) and mitochondria coverage (E) in SF1 neurons from *Ucp2KO* mice injected with either saline or glucose (ip, 2 g/kg BW). n (*Ucp2KO* mice with ip saline) = 395 mitochondria/17 cells/3 mice; n (*Ucp2KO* mice with ip glucose) = 437 mitochondria/19 cells/3 mice.

F-H: Cumulative probability distribution of cross-sectional mitochondria area (F), Mitochondria density (G) and mitochondria coverage (H) in SF1 neurons from *Ucp2KOKI^{Sf1}* mice injected with either saline or glucose (ip, 2 g/kg BW). n (*Ucp2KOKI^{Sf1}*mice with ip saline) = 464 mitochondria/19 cells/3 mice; n (*Ucp2KOKI^{Sf1}* mice with ip glucose) = 657 mitochondria/21 cells/4 mice.

I-K: Cumulative probability distribution of cross-sectional mitochondria area (I), mitochondria density (J) and mitochondria coverage (K) in SF1 neurons of *Ucp2KI^{Sf1}* mice injected with either saline or glucose (ip, 2 g/kg BW). n (*Ucp2KI^{Sf1}* mice with ip saline) = 486 mitochondria/20 cells/4 mice; n (*Ucp2KI^{Sf1}* mice with ip glucose) = 491 mitochondria/21 cells/4 mice.

All data represent the mean±SEM *=$p<0.05$; **=$p<0.01$; ***=$p<0.001$ compared to their saline group. See also Figure S1 and Figure S2.
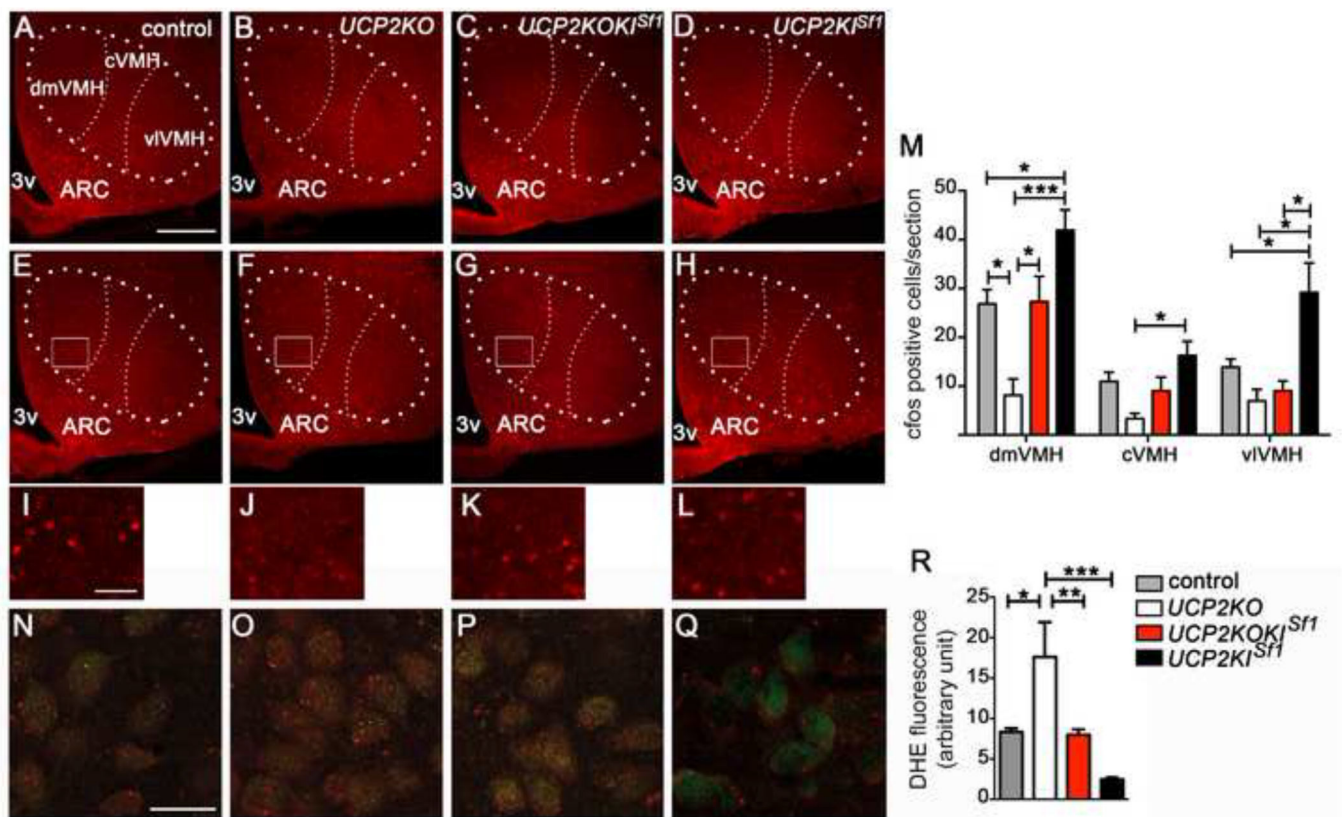
Figure 3.
UCP2 is required for the regulation of neuronal activity and ROS production

A-D: Representative micrographs showing immunofluorescent c-fos staining in the VMH of control (A), *Ucp2KO* (B), *Ucp2KOKI^Sf1* (C) and *Ucp2KI^Sf1* mice (D) after 1 hour from peripheral saline administration.

E-H: Representative micrographs showing immunofluorescent c-fos staining in the VMH of control (E), *Ucp2KO* (F), *Ucp2KOKI^Sf1* (G) and *Ucp2KI^Sf1* mice (H) after 1 hour from peripheral glucose administration (2g/kg BW).

Bar scale in A (for A-H) represents 200 μm. 3v= third ventricle; dmVMH= dorsomedial subdivision of the ventromedial nucleus; cVMH= central subdivision of the ventromedial nucleus; vlVMH= ventrolateral subdivision of the ventromedial nucleus; ARC=arcuate nucleus.

I-L: High power images from boxed areas in panels E-H showing c-fos staining in the VMH of control (I), *Ucp2KO* (J), *Ucp2KOKI^Sf1* (K) and *Ucp2KI^Sf1* mice (L) after 1 hour from peripheral glucose administration (2g/kg BW). Bar scale in I (for I-L) represents 50 μm.

M: Quantification of c-fos expression in the dorsomedial (dmVMH), central (cVMH) and ventrolateral (vlVMH) subdivisions of the VMH of control mice (n=4), *Ucp2KO* mice (n=4), *Ucp2KOKI^Sf1* mice (n=4) and *Ucp2KI^Sf1* mice (n=4) after peripheral glucose (2g/kg BW) administration.

N-Q: Representative micrographs showing fluorescent DHE (red) in dmVMH SF1 neurons (green) of control (N), *Ucp2KO* (O), *Ucp2KOKI^Sf1* (P) and *Ucp2KI^Sf1* mice (Q). Scale bar in N (for N-Q) represents 25 μm.

R: Quantification of DHE intensity in SF1 neurons of control mice (n=4), *Ucp2KO* mice (n=5), *Ucp2KOKI*^{Sf1} (n=5) and *Ucp2KI*^{Sf1} mice (n=6).

All data represent the mean±SEM. *=p<0.05; **=p<0.01; ***=p<0.001.
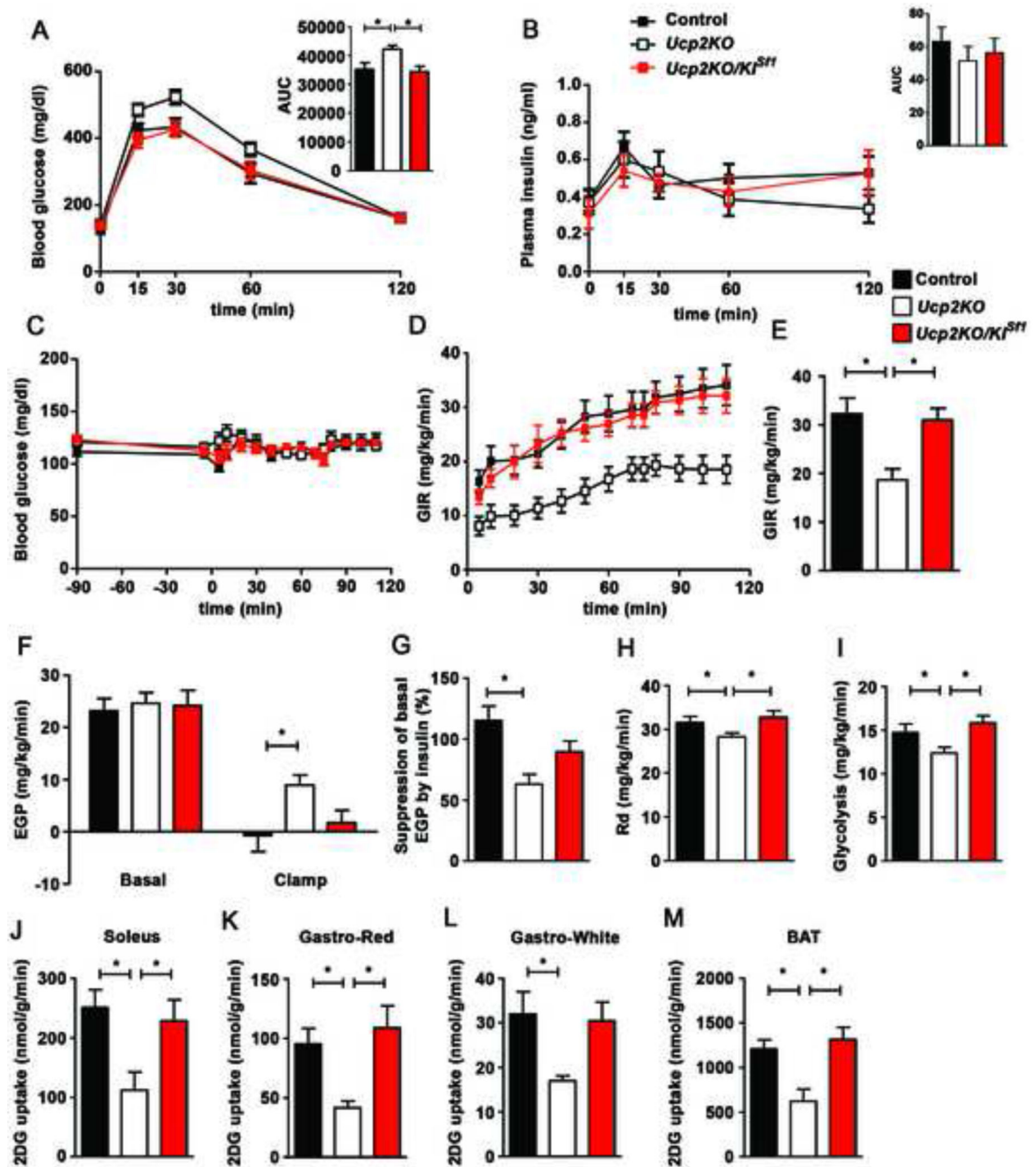
Figure 4. UCP2 in SF1 neurons is required to control insulin sensitivity in the liver, muscle and brown adipose tissue

A: Glucose tolerance test (GTT) in male control (n=13), *Ucp2KO* (n=14) and *Ucp2KOKI^Sf1* mice (n=8).

B: Plasma insulin concentration during GTT in male control (n=9), *Ucp2KO* (n=6) and *Ucp2KOKI^Sf1* mice (n=6).

C: Blood glucose levels during hyperinsulinemic-euglycemic clamp studies in control, *Ucp2KO* and *Ucp2KOKI^Sf1* mice (n=8 per each experimental groups).

D: Graph showing glucose infusion rate (GIR) required to maintain euglycemia during the clamp period in control, *Ucp2KO* and *Ucp2KOKI^Sf1* mice (n=8 per each experimental groups).

E: Graph showing the average GIR between 70 and 115 min in control, *Ucp2KO* and *Ucp2KOKI^Sf1* mice (n=8 per each experimental groups).

F: Endogenous glucose production (EGP) during both basal and clamp period in control, *Ucp2KO* and *Ucp2KOKI^Sf1* mice (n=8 per each experimental groups).

G: Graph showing the percent suppression levels of EGP induced by insulin infusion in control, *Ucp2KO* and *Ucp2KOKI^Sf1* mice (n=8 per each experimental groups).

H: Graph showing the rate of glucose disappearance (Rd) during the clamp period, which represents whole body glucose utilization, in control, *Ucp2KO* and *Ucp2KOKI^Sf1* mice (n=8 per each experimental groups). Basal Rd is equal to basal EGP.

I: Graph showing the rates of whole body glycolysis in control, *Ucp2KO* and *Ucp2KOKI^Sf1* mice (n=8 per each experimental groups).

J-M: Graphs showing 2-[^{14}C]-Deoxy-D-Glucose (2DG) uptake in soleus (J), red (Gastro-Red; K) and white (Gastro-White; L) portions of the gastrocnemius and brown adipose tissue (BAT; M) during the clamp period in control, *Ucp2KO* and *Ucp2KOKI^Sf1* mice (n=8 per each experimental groups).

Data in all graphs represent the mean±SEM. *=$p<0.05$. See also Figure S3 and Figure S4.
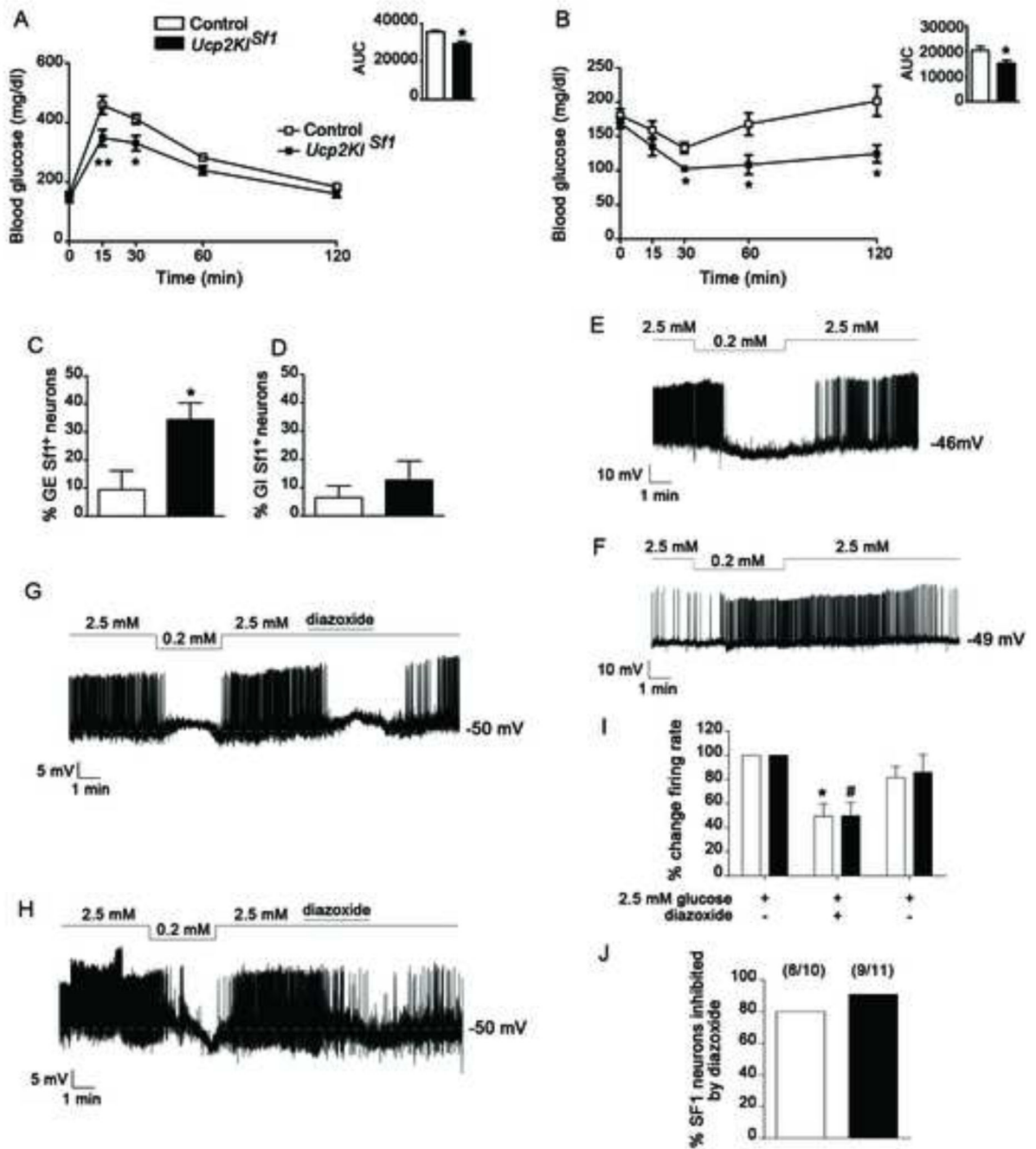
Figure 5. UCP2 overexpression selectively affects VMH GE neurons
A-B: Graphs showing results from glucose tolerance test (GTT; ip, 2g/kg BW glucose; A), and insulin tolerance test (ip, 1U/kg BW insulin; B), of control (n=7-9) and $Ucp2KI^{Sf1}$ mice (n=7-9).

C-D: Graphs showing the percent of glucose-excited (GE; C) and glucose-inhibited (GI; D) in SF1 neurons of control (n=7) and $Ucp2KI^{Sf1}$ (n=8) mice.

E-F: Representative tracers from a GE (E) and a GI (F) neuron from an $Ucp2KI^{Sf1}$ mouse and a control mouse, respectively.

G-H: Representative tracers of GE neurons from control (G) and *Ucp2KI*^{Sf1} mice (H), respectively, showing that their responses to glucose are dependent of K_{ATP} channels.

I: Graph showing the percent change of firing rate of dmVMH GE neurons after the addition in the media of diazoxide (300 µM), a K_{ATP} channel opener. n=10 cells/5 control mice; n=11 cells/5 *Ucp2KI*^{Sf1} mice.

J: Graph showing the percent of SF1-GE neurons in the dmVMH of control (8 cells out of 10 in 5 mice total) and *Ucp2KI*^{Sf1} mice (9 cells out of 11 in 5 mice total) that were inhibited by diazoxide (300 µM).

All data represent the mean±SEM. Panels A-C: *=p<0.05 and **=p<0.01 compared to control mice.; Panel I: *=p<0.05 compared to control in 2.5 mM glucose; #=p<0.05 compared to *Ucp2KI*^{Sf1} in 2.5 mM glucose.
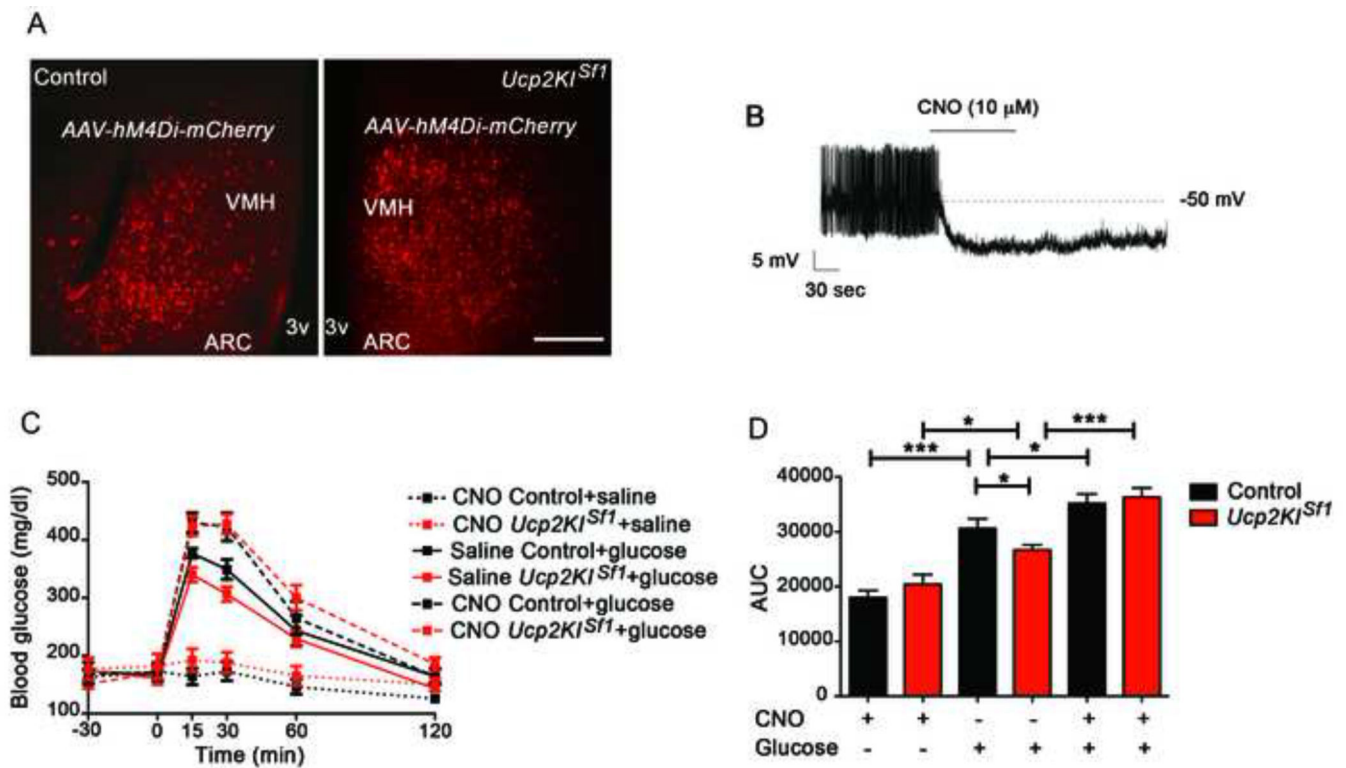
Figure 6. UCP2-regulated VMH neuronal activation is critical for the control of whole body glucose metabolism

A: Representative micrographs of the injection site of the *AAV-hM4Di-mCherry* in control (left panel) and *Ucp2KI^{Sf1}* mice (right panel).

B: Representative recording showing decreased firing rate of a neuron from an *Ucp2KI^{Sf1}* mouse infected with *the AAV-hM4Di-mCherry* upon 10 μM CNO application.

C: Graph showing the changes in blood glucose levels after 2g/kg BW ip. glucose injection given 30 minutes after either CNO (ip, 0.3 mg/kg BW) or vehicle injection in control and *Ucp2KI^{Sf1}* mice expressing *AAV-hM4Di-mCherry* in the VMH (n=6-7 mice per group).

D: Graph showing the results of the area under the curve (AUC) of the GTT showed in panel C.

All data represent the mean±SEM. *=p<0.05; ***=p<0.001. Bar scale in the right panel of A (and for the left panel) represents 200 μm. VMH= ventromedial nucleus; ARC= arcuate nucleus; 3v= third ventricle. See also Figure S5.